A Simulation Perspective: The Potential and Limitation of Ge GAA CMOS Devices

Sheng-Kai Su[1], Edward Chen[1], and Jeff Wu[2]
1 Corporate Research, 2 TCAD Division,
Taiwan Semiconductor Manufacturing Company, Ltd.
No. 168, Park Ave. 2, Hsinchu Science Park, Hsinchu County, Taiwan
E-mail: sksua@tsmc.com

***Abstract*—The electrical characteristics of <110> n/p Ge nanowire transistors (NWTs) with the cross section of 6×6nm² have been studied. The I_{ON} performance and the subthreshold swing are simulated by multi-subband Boltzmann transport equation and ballistic quantum transport solvers, respectively. The performance of <110> nGe NWTs is sensitive to the barrier height of interfacial layer due to highly-anisotropic Λ-valleys. The dimension-dependent *k·p* parameters based on tight-binding full band are used to address the strong confinement of pGe NWTs. Comparing to Si NWTs, the intrinsic I_{ON} is twice as high for both n/p Ge NWTs at 28nm channel length. As the channel length is scaled down, such I_{ON} benefit is maintained till the tunneling effect comes in and degrades the subthreshold swing.**

Keywords-Ge, nanowire, interfacial layer, ballistic ratio, source-to-drain tunneling, CMOSFETs

I. INTROUDUCTION

Germanium (Ge) is one of the promising materials for CMOS technology due to its high electron and hole mobilities. The highly anisotropic Λ valleys with multiple degenerate states also provide sufficient density-of-states (DOS) in Ge nFETs, which is not the case in III-V devices. The only problem is that the small bandgap in Ge results in large band-to-band tunneling (BTBT) leakage at the OFF state [1]. To solve the issue, the gate-all-around (GAA) structure is used to enlarge the effective bandgap. After geometrical quantum confinement with 6×6nm² square cross section, the direct BTBT (*i.e.*, $\Gamma_v \rightarrow \Gamma_c$) would be largely suppressed since the small effective mass at Γ valley (*i.e.*, $m^*=0.048m_0$) results in large direct bandgap after quantum confinement and the indirect BTBT should be in the acceptable range since the indirect bandgap (*i.e.*, $\Gamma_v \rightarrow \Lambda$) approaches to 1eV. Therefore, the device performance and the gate length scalability will be the next questions to answer. In this article, we simulate <110> Ge nanowire transistors (NWTs) with 6×6nm² cross section. The multi-subband Boltzmann transport equation (MSBTE) with the major scattering mechanisms in MOSFETs is used to estimate ON state performance [2]. The ballistic quantum transport solver is applied for addressing the source-to-drain tunneling (SDT) current [2, 3]. In addition, the finite barrier height between interfacial layers (ILs) and semiconductor interface is considered for conduction band in nNWTs. The dimension-dependent *k.p* parameters are used for valence band in pNWTs. The simulated transfer characteristics of Ge NWTs show ~2×I_{ON} of Si NWTs achieved for both nFET and pFET. Furthermore, the ballistic ratio (BR) is extracted and compared with the experiments in order to validate our scattering assumption and prediction power. Finally, we examine the scalability of Ge NWTs with the subthreshold swing degradation due to SDT and the result is also compared with the case of Si NWTs.

II. SIMULATION METHODOLOGY

TABLE I. BAND PARAMETERS USED IN SIMULATIONS FOR GERMANIUM NANOWIRE.

Electron:	
m_l_Δ [m_0]	0.952
m_t_Δ [m_0]	0.202
α_Δ [eV^{-1}]	0.38
m_l_Λ [m_0]	1.588 [4]
m_t_Λ [m_0]	0.08152 [4]
α_Λ [eV^{-1}]	0.27
m_Γ [m_0]	0.048
α_Γ [eV^{-1}]	1
Hole (<110> 6×6nm²):	
γ_1	11.56
γ_2	3.24
γ_3	4.91
Δ_{SO} [eV]	0.29

In the work, the electron and hole transport are solved by MSBTE and Poisson equation self-consistently [2]. The effective mass and nonparabolicity of the different conduction valleys (*i.e.*, Λ, Δ, Γ) are extracted from the bandstructure and DOS simulated by empirical pseudopotential method [5, 6]. For the valence band, the three-band *k·p* parameters for the specific wire geometry are obtained by fitting the results of tight-binding method [7]. The extracted band parameters are listed in Table I. Since Ge possesses highly anisotropic effective masses at Λ valley, the eigen-energy states between with and without considering wavefunction penetration into ILs [8] are different especially for <110> Ge nNWTs. Therefore, the band offsets and oxide effective masses derived from the gate tunneling experiments [9, 10] are used to calculate the eigen-energy for the different ILs applied on Ge nNWTs. To simplify our simulation, no interface trap density between ILs and Ge is considered (*i.e.*, D_{it}=0). For the

dissipative transport simulation, we include scattering mechanisms of acoustic phonon, optical phonon, surface roughness, and ionized impurity. The scattering parameters related to bulk are obtained from Ref. [11]. The parameters affected by ILs (*i.e.*, D_{ac}, Δ_{sr}, Λ_{sr}) are obtained by fitting the long change mobility vs. inversion charge density and temperature in Si FinFETs [7]. In our simulation, Si NWTs and Si FinFETs share the same scattering parameters. For Ge NWTs, we keep the same roughness parameters (*i.e.*, Δ_{sr}, Λ_{sr}) as that of Si. The acoustic deformation potential (*i.e.*, D_{ac}) of Ge NWTs is obtained by keeping the D_{ac} ratio between Si and Ge bulks [11]. For the quantum transport simulation, quantum transmitting boundary method (QTBM) is used to calculate the transmission coefficient under the barrier. Afterwards, the transmission coefficient is replaced by the position-dependent generation and recombination rates for SDT current calculation [2]. To validate the methodology, the ballistic IV characteristics are compared with the IV obtained by $sp^3d^5s^*$ non-equilibrium Green's function (NEGF) [3]. Since both results show a good agreement and the computational cost in effective mass approximation (EMA) QTBM is cheaper than that in $sp^3d^5s^*$ NEGF, the SDT effect shown in the work is calculated by EMA QTBM.

III. Result and Discussion

Fig. 1 compares the subband structures of 6×6nm^2 <110> nGe NWTs for closed (*i.e.*, infinite barrier height) and open boundary (*i.e.*, finite barrier height) conditions at Ge/IL interface.

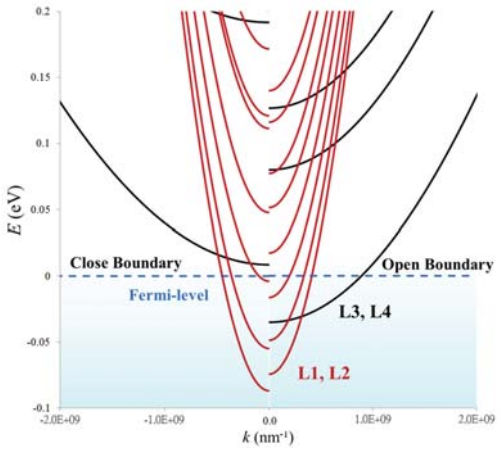

Fig.1 The bandstructure of 6×6nm^2 <110> nGe NWTs for closed (*i.e.*, infinite barrier height) and open boundary (*i.e.*, finite barrier height) conditions at Ge/IL interface. There are two groups of valleys named L1,L2 (red): low transport and high confinement masses; L3,L4 (black): high transport and low confinement masses. The fermi-level is at zero energy and the charge density for both cases are around 5e12 cm^{-2}. For the open boundary, the ground state energy of L3,L4 valleys becomes lower than the Fermi-level, which increases the population of L3,L4 valleys. This effect arises because of the highly anisotropic Ge conduction band at Λ (m_l=1.59 m_0 and m_t=0.082 m_0).

There are two groups of valleys named L1, L2 (red): low transport and high confinement masses; L3, L4 (black): high transport and low confinement masses. The fermi-level is at zero energy and the charge density for both cases are around 5e12 cm^{-2}. For the open boundary condition, the ground state energy of L3, L4 valleys becomes lower than the Fermi-level, which is not seen for the closed boundary condition. The difference comes from the nature of highly anisotropic Λ valley in Ge (m_l=1.59 m_0 and m_t=0.082 m_0). Since the subbands with the lighter confinement effective mass would have stronger "communications" with ILs ($^1/_{m_{ox}}\left(^{\partial\psi_{ox}}/_{\partial x}\right) = {}^1/_{m_s}\left(^{\partial\psi_s}/_{\partial x}\right)$), the obvious difference is shown in Fig. 1. This change would further modify the population of different valleys and affect the averaged effective mass and ballistic velocity. Fig. 2 shows the IV characteristics of nGe NWTs with different ILs at V_{DS}=0.7V. We consider low-barrier IL (red), high-barrier IL (black), and with closed boundary condition (dash) in Fig. 2. The energy discontinuity at IL/Ge interface used for low-barrier IL and high-barrier IL are ~1 eV and ~3 eV, respectively. The Ge NWTs with low-barrier IL shows higher current than that with high-barrier IL. The main reason is that the wire with low-barrier IL has more inversion charge density than that with high-barrier IL due to denser subbands as shown in Fig. 1. We also check the velocity for these cases. Although the wire with low-barrier IL has the smaller ballistic velocity than that with high-barrier ILs, the "spread" of the wavefunction in the wire with low-barrier IL mitigates phonon and surface roughness scatterings and eventually both cases have the comparable injection velocities.

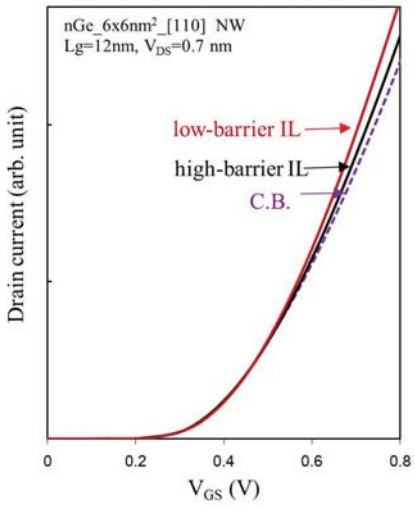

Fig.2 The transfer characteristics of 6×6nm^2 <110> nGe NWTs at V_{DS}=0.7V for low-barrier IL (red), high-barrier IL (black), and with close boundary (C.B.) condition (dash). The energy discontinuity at IL/Ge interface used for low-barrier IL and high-barrier IL are ~1 eV and ~3 eV respectively.

The intrinsic (*i.e.*, R_{ext}~0) I_D-V_{GS} with V_{DS}=0.7V for both 6×6nm^2 <110> n/p Ge (red) and Si (black) NWTs at L_G=28nm are shwon in Fig. 3. Both n and p Ge NWTs show ~2× I_{ON} comparing to Si NWTs at the same I_{OFF}. The Ge pNWT even outperforms the Si nNWT although the long channel mobility of the Ge pNWT is lower than that of the Si nNWT. This is

attributed to the high ballistic velocity in the Ge pNWT. Since the inversion charge density in the Ge nNWT is comparable to that in the Si nNWT, the high ballistic velocity of the Ge nNWT again beats that of the Si nNWT.

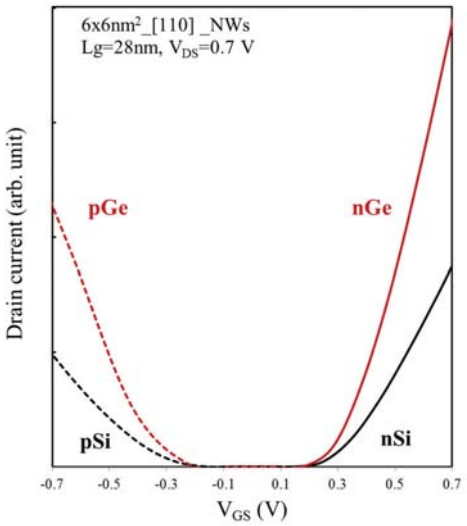

Fig.3 Simulated I_D-V_{GS} with V_{DS}=0.7V for both 6×6nm^2 <110> n/p Ge (red) and Si (black) NWTs at channel length=28nm. Both n and p Ge NWTs show ~2× I_{ON} comparing to Si NWTs at the same I_{OFF}.

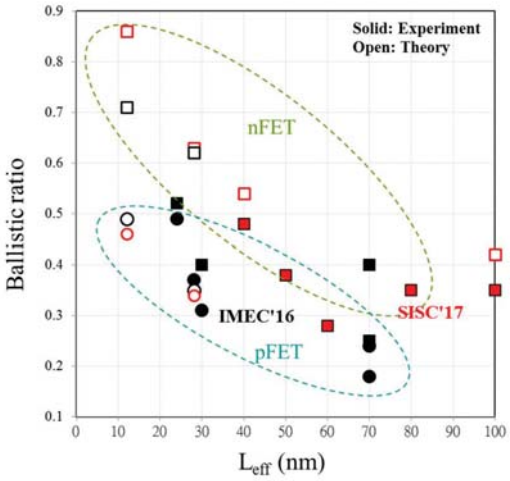

Fig.4 Ballistic ratio of n (square) / p (circle) Ge (red) and Si (black) NWTs versus effective channel length L_{eff}. The simulation results are empty symbols with dimension 6×6nm^2, and the results extracted from experiments are solid symbols: n/p Si NWTs are from Ref. [12] with diameter ~8nm, and nGe NWTs are from Ref. [13] with dimension ~10×40nm^2.

In order to validate our scattering assumption and our prediction power, we compare the simulated BR with experimental BR [12, 13]. Fig. 4 shows the BR of n (square) / p (circle) Ge (red) and Si (black) NWTs versus effective channel length L_{eff}. The simulation results are empty symbols with dimension 6×6nm^2. The results extracted from experiments are solid symbols: n/p Si NWTs are from Ref. [12] with diameter ~8nm, and nGe NWTs are from Ref. [13] with dimension ~10×40nm^2. The BR of nFET is higher than that of pFET, and the BR of both n and p devices increase as L_{eff} decreases. Fig. 4 shows that our simulations follow the trend lines well. Although the scattering parameters are extracted from the long channel mobility of Si FinFETs, we find that our model can capture the device I-V (not shown here [14]) and BR well for both Si and Ge NWTs without tuning any scattering parameters. Our simulation even shows that nGe NWTs with L_{eff}=12nm is approaching to ballistic transport due to the long backscattering mean-free-path and short critical length [15].

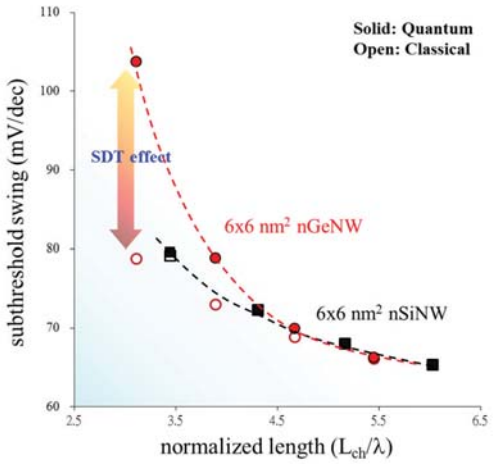

Fig.5 The subthreshold swing as a function of the normalized length, which is defined by the channel length L_{ch} deviding by the nature length λ [16], for nGe (circle) and nSi (square) NWTs. The quantum and classical treatments of electron transport are solid and empty symbols respectively. Ge NWTs show stronger direct source-to-drain tunneling (SDT) than Si NWTs due to the lower bandedge mass.

From the BR point of view, Ge NWTs enjoy the benefit from gate length scaling over Si NWTs. However, the electrostatic control and SDT could decline the benefits. Fig. 5 shows the subthreshold swing versus the normalized gate length for 6×6nm^2 Ge (circle) and Si (square) nNWTs. The normalized gate length is defined by the channel length L_{ch} deviding by the nature length λ [16]. The quantum and classical treatments of electron transport are solid and empty symbols, respectively. For the classical treatment, the subthreshold swing of Ge and Si nNWTs are similar at the same normalized length because the difference between the dielectric constants of Ge and Si is compensated. However, the quantum treatment shows that the subthreshold swing of Ge nNWTs increases exponentially as the channel length scales down, which is unapparent in Si nNWTs. The SDT current under the barrier contributes the difference, which is caused by the low transport mass (~0.09 m_0) at the band edge of <110> Ge NWTs [17].

IV. Conclution

Energy discontinuity at IL/Ge interface has significant impact on device performance especially for nGeNWTs. The smaller energy discontinuity at IL/Ge interface delivers better performance for the ideal gate dielectric interface. Based on the thoroughgoing band parameters and the scattering parameters calibrated by the long channel mobility of Si FinFETs, our model captures BR and IV characteristics well for both n/p Ge and Si NWTs. Ge GAA CMOS shows twice the intrinsic I_{ON} of Si GAA CMOS at 28nm channel length. As the channel length scales down, the striking I_{ON} benefit is maintained till the source-to-drain tunneling current dominates the subthreshold swing.

Acknowledgment

We thank Gerben Doornbos, Mark van Dal, and Aryan Afzalian for insightful technical discussions.

References

[1] M.J.H. van Dal, G. Vellianitis, B. Duriez, G. Doornbos, C.-H. Hsieh, B.-H. Lee, K.-M. Yin, M. Passlack, C.H. Diaz, "Germanium p-channel FinFET fabricated by aspect ratio trapping," IEEE Trans. Electron Dev., vol. 61, pp. 430-436, 2014.

[2] Global TCAD Solutions MinimosNT User manual, 2017.

[3] NEMO5 User manual, 2015.

[4] T.P.McLean, and E.G.S. Paige, "Electron-hole scattering and minority carrier mobility in germanium," J. Phy. Chem. Solids, vol. 18, pp. 139-149, 1961.

[5] J.R. Chelikowsky and M.L. Cohen, "Nonlocal pseudopotential calculations for the electronic structure of eleven diamond and zinc-blende semiconductors," Phys. Rev. B, vol. 14, pp. 556-582, 1976.

[6] M. M. Rieger and P. Vogl, "Electronic-band parameters in strained $Si_{1-x}Ge_x$ alloys on $Si_{1-y}Ge_y$ substrates," Phys. Rev. B, vol. 48, pp. 14276-14287, 1993.

[7] E. Chen, S.K. Su, and J. Wu, "$Si_{1-x}Ge_x$ thin-layer hole mobility based on thickness-dependent 6×6k.p parameters,"in SISC abstract book, 5.13, 2017.

[8] P. Harrison, *Quantum wells, wires and dots: Theoretical and computational physicsof semiconductor nanostructures,* John Wiley & Sons, 3rd ed., 2011.

[9] P.S. Goley, and M.K. Hudait, "Germanium based field-effect transistors: Challenges and opportunities," Materials, vol. 7, pp. 2301-2339, 2014.

[10] A.V. Shaposhnikov, T.V. Perevalov, V.A. Gritsenko, C.H. Cheng, and A. Chin, "Mechanism of GeO_2 resistive switching based on the multi-phonon assisted tunneling between traps," Appl. Phys. Lett., vol. 100, id. 243506, 2012.

[11] C. Jacoboni, F. Nava, C. Canali, and G. Ottaviani, "Electron drift velocity and diffusivity in germanium," Physical Review B 24.2, 1014, 1981.

[12] R. Ritzenthaler *et al.*, PTW presentation, IMEC, 2016.

[13] W. Chung, H. Wu, M. Si, and P. D. Ye, "Experimental extraction of Ballistic Efficiency of Germanium Nanowire NMOSFETs," in SISC abstract book, 5.1, 2017.

[14] M.J.H. van Dal, G. Vellianitis, G. Doornbos, B. Duriez, M. Holland, T. Vasen, A. Afzalian, E. Chen, S.K. Su, T.K. Chen, T.M. Shen, Z.Q. Wu, C.H. Diaz, "Ge CMOS gate stack and contact development for vertically stacked lateral nanowire FETs," *submitted to IEDM 2018*.

[15] M. Lundstrom, "Elementary scattering theory of the Si MOSFET," IEEE Electron Device Lett., vol. 18, pp. 361-363, 1997.

[16] I. Ferain, C.A. Colinge, and J.P. Colinge, "Multigate transistors as the future of classical metal–oxide–semiconductor field-effect transistors," Nature vol. 479, pp. 310-316, 2011.

[17] S.R Mehrotra, S.Kim, T.Kubis, M.Povolotskyi, M. Lundstrom, and G. Klimeck, "Engineering Nanowire n-MOSFETs at L_g<8nm," IEEE Trans. on Electron Dev., vol. 60, pp. 2171-2177, 2013.